Effect of Changing Heart Rate on the Ocular Pulse and Dynamic Biomechanical Behavior of the Optic Nerve Head

Yuejiao Jin,[1,2] Xiaofei Wang,[3] Sylvi Febriana Rachmawati Irnadiastputri,[2] Rosmin Elsa Mohan,[2,4] Tin Aung,[4,5,6] Shamira A. Perera,[4,5] Craig Boote,[2,10] Jost B. Jonas,[11] Leopold Schmetterer,[4,5,7–9] and Michaël J.A. Girard[2,4]

[1]National University of Singapore Graduate School for Integrative Sciences and Engineering, National University of Singapore, Singapore
[2]Department of Biomedical Engineering, National University of Singapore, Singapore
[3]Beijing Advanced Innovation Center for Biomedical Engineering, School of Biological Science and Medical Engineering, Beihang University, Beijing, China
[4]Singapore Eye Research Institute, Singapore National Eye Centre, Singapore
[5]Duke-National University of Singapore Medical School, Singapore
[6]Department of Ophthalmology, Yong Loo Lin School of Medicine, National University of Singapore, Singapore
[7]Lee Kong Chian School of Medicine, Nanyang Technological University, Singapore
[8]Department of Clinical Pharmacology, Medical University of Vienna, Vienna, Austria
[9]Center for Medical Physics and Biomedical Engineering, Medical University of Vienna, Vienna, Austria
[10]School of Optometry & Vision Sciences, Cardiff University, Cardiff, United Kingdom
[11]Department of Ophthalmology Medical Faculty Mannheim, Heidelberg University, Mannheim, Germany

Correspondence: Michaël J.A. Girard, National University of Singapore, Engineering Block 4, #04-8, 4 Engineering Drive 3, Singapore, 117583; mgirard@nus.edu.sg.

YJ and XW contributed equally.

Received: September 16, 2019
Accepted: January 15, 2020
Published: April 21, 2020

Citation: Jin Y, Wang X, Irnadiastputri SFR, et al. Effect of changing heart rate on the ocular pulse and dynamic biomechanical behavior of the optic nerve head. *Invest Ophthalmol Vis Sci.* 2020;61(4):27. https://doi.org/10.1167/iovs.61.4.27

Purpose. To study the effect of changing heart rate on the ocular pulse and the dynamic biomechanical behavior of the optic nerve head (ONH) using a comprehensive mathematical model.

Methods. In a finite element model of a healthy eye, a biphasic choroid consisted of a solid phase with connective tissues and a fluid phase with blood, and the lamina cribrosa (LC) was viscoelastic as characterized by a stress-relaxation test. We applied arterial pressures at 18 ocular entry sites (posterior ciliary arteries), and venous pressures at four exit sites (vortex veins). In the model, the heart rate was varied from 60 to 120 bpm (increment: 20 bpm). We assessed the ocular pulse amplitude (OPA), pulse volume, ONH deformations, and the dynamic modulus of the LC at different heart rates.

Results. With an increasing heart rate, the OPA decreased by 0.04 mm Hg for every 10 bpm increase in heart rate. The ocular pulse volume decreased linearly by 0.13 µL for every 10 bpm increase in heart rate. The storage modulus and the loss modulus of the LC increased by 0.014 and 0.04 MPa, respectively, for every 10 bpm increase in heart rate.

Conclusions. In our model, the OPA, pulse volume, and ONH deformations decreased with an increasing heart rate, whereas the LC became stiffer. The effects of blood pressure/heart rate changes on ONH stiffening may be of interest for glaucoma pathology.

Keywords: ocular biomechanics, ocular pulse, heart rate, optic nerve head, finite element analysis

Glaucoma is a complex, multifactorial disease. Although the pathogenic mechanism of glaucoma has still not been well understood, it has generally been accepted that various interlinked biomechanical and vascular pathways to glaucomatous injury are involved, and that these are closely related to the optic nerve head (ONH) biomechanics.[1–8] The ONH, and in particular the lamina cribrosa (LC), is a primary site of interest during the development of glaucoma because it is the region where retinal ganglion cell (RGC) axon damage occurs. Because the ONH is constantly exposed to several loads in vivo (e.g., IOP, cerebrospinal fluid pressure [CSFP], orbital fat pressure, optic nerve traction),[6,9–13] there is a general consensus that knowing how "robust" an ONH is could be critical information for estimating the risk of developing glaucoma.

To date, to assess the biomechanics of the ONH in vivo, the typical approach has been to artificially manipulate IOP (e.g., with ophthalmodynamometry), whereas observing the resulting deformations with optical coherence tomography (OCT).[14–17] Although such methods may have value from a research point of view, they may not be easily translated clinically owing to discomfort during the examination of the

Investigative Ophthalmology & Visual Science

patients. However, IOP is not constant but rather pulsatile, fluctuating constantly with the cardiac cycle. The fluctuation of IOP with the heart rate has been known as the ocular pulse, and the difference between the systolic and diastolic IOP has been termed the ocular pulse amplitude (OPA). In a previous study, we proposed a framework to assess ONH biomechanics in vivo without artificially manipulating IOP. ONH deformations can indeed be measured by using the ocular pulse as the load,[18] and from such data, modeling can help us interpret these deformation data to derive stiffness estimates for the ONH.[19]

This is, however, a complex engineering problem: the ONH tissues are viscoelastic,[7,20,21] which basically means that ONH stiffness is affected by the rate of loading, or in other words, the duration of the cardiac cycle. Indeed, collagenous soft tissues typically appear stiffer when they are loaded faster. This is a protective mechanism for soft tissues to handle highly dynamic events.[7,20] Furthermore, it has been shown clinically that an increase in heart rate or a change in blood pressure can also affect the OPA[22,23]; this will in turn affect the deformations of the ONH.

To measure the stiffness of the ONH using the ocular pulse as a natural load, we believe it is critical to first build an understanding of how the heart rate and blood pressure change the IOP (i.e., the OPA), and how they also affect the stiffness and deformations of the ONH tissues. From a clinical point of view, if ONH tissues appear stiffer, a physician should be able to tell whether this is because of a different heart rate/blood pressure, or because of tissue remodeling from glaucoma. In this study, we aim to build such an understanding using finite element (FE) modeling. In the future, our proposed models could be combined with experimental data to assess ONH stiffness in vivo.

Methods

Using FE modeling, we previously modeled the origin of the ocular pulse and its effect on the ONH.[19] We found that a change in arterial pressure (as that occurring from diastole to systole) resulted in choroidal swelling, which in turn induced a change in IOP (the OPA) because of the incompressibility of the vitreous. Both the OPA and choroidal swelling were responsible for deforming the ONH tissues, and a relatively large shearing of neural tissues was observed within the neuroretinal rim. The vast majority of the trends we reported matched clinical and experimental data.

In this study, we used the same model, but we further defined the LC as a viscoelastic material. Such viscoelastic properties were obtained experimentally using uniaxial stress relaxation tests. Using our FE model, we then varied the heart rate from 60 to 120 bpm and studied its effect on (1) the OPA, (2) the choroidal pulse volume, (3) ONH deformations, and (4) LC stiffness.

Three-Dimensional Geometry of the Ocular and Orbital Tissues

The geometry of the three-dimensional eye model was adapted from our previous studies.[12,19,24] In summary, the eye globe and optic nerve were reconstructed from magnetic resonance imaging scans of a heathy subject. The corneoscleral shell was assumed to be spherical, with an outer diameter of 24 mm and thickness of 1 mm. The optic nerve was composed of three tissues: the nerve tissue, the pia mater, and the dura mater. A generic ONH geometry was constructed and embedded within the corneoscleral shell, including the scleral flange, Bruch's membrane, the LC, the prelaminar tissue, and the border tissue of Elschnig and Jacoby as extensions of the pia mater. The model was then meshed using 67,584 eight-node hexahedrons and 3024 six-node pentahedrons (Fig. 1). The mesh density was numerically validated through a convergence test. The whole eye was reconstructed, and symmetry conditions were not applied.

Biomechanical Properties of the Ocular Tissues

The sclera was modeled as a fiber-reinforced composite, as described in our previous article.[25] The neural tissues and Bruch's membrane were modeled as isotropic elastic materials.[26] Notice that the isotropic elastic material used is a modified version of the linear elastic material, which can be applied to nonlinear deformation. The hyperelastic strain-energy function[27,28] is shown in the following:

$$W = \frac{1}{2}\lambda(\mathrm{tr}\mathbf{E})^2 + \mu\mathbf{E} : \mathbf{E} \quad (1)$$

where E represents the Green-Lagrangian tensor, and the material coefficients λ and μ are known as the Lamé parameters. The pia and dura were modeled as Yeoh materials, as characterized from experiments with porcine eyes.[24] As performed in our previous study, we modeled the choroid as a biphasic material comprising a solid phase and a fluid phase (i.e., blood) to allow for changes in blood pressure during the cardiac cycle and the movement of blood within the choroid.[19] All biomechanical parameters are listed in Table 1.

Viscoelastic Properties of the LC

To characterize the response of the LC under dynamic loading, such as the heart rate, we studied its viscoelastic properties. Because the viscoelasticity properties of the LC have not been reported in the literature yet, we conducted uniaxial stress relaxation tests of the LC of seven porcine eyes.

Experiments were performed in accordance with the ARVO Statement for the Use of Animals in Ophthalmic and Vision Research. The experimental procedure followed the previously described methodology designed for the sclera.[29,30] In brief, seven fresh porcine eyes were collected and cleaned of all extraorbital tissues. Note that the sex and age information of the animals were not available. After dissecting the eye and cutting the optic nerve, the retina and choroidal layers were removed. A customized device was used to cut a scleral strip (orientation: inferior to superior) with the LC in its center (width: 1.2 mm; Fig. 2). Mineral oil was applied to the specimen surface to maintain hydration. Each sample was mounted between the two grips of the uniaxial tensile tester (Instron 5848; Instron, Inc., Norwood, MA, USA) with the LC exposed in the center (Fig. 2c). The length of each LC specimen (grip-to-grip distance) was measured with an electronic Vernier caliper (mean: 2.14 mm) before each uniaxial test. The average aspect ratio of the LC specimens was 1.78, which was adequate for the uniaxial tests. Typical aspect ratios for scleral specimens were approximately 2:1 to avoid artifacts.[31,32] The sample was subjected to 10 cycles of preconditioning at 1% strain prior to the stress relaxation test. The sample was

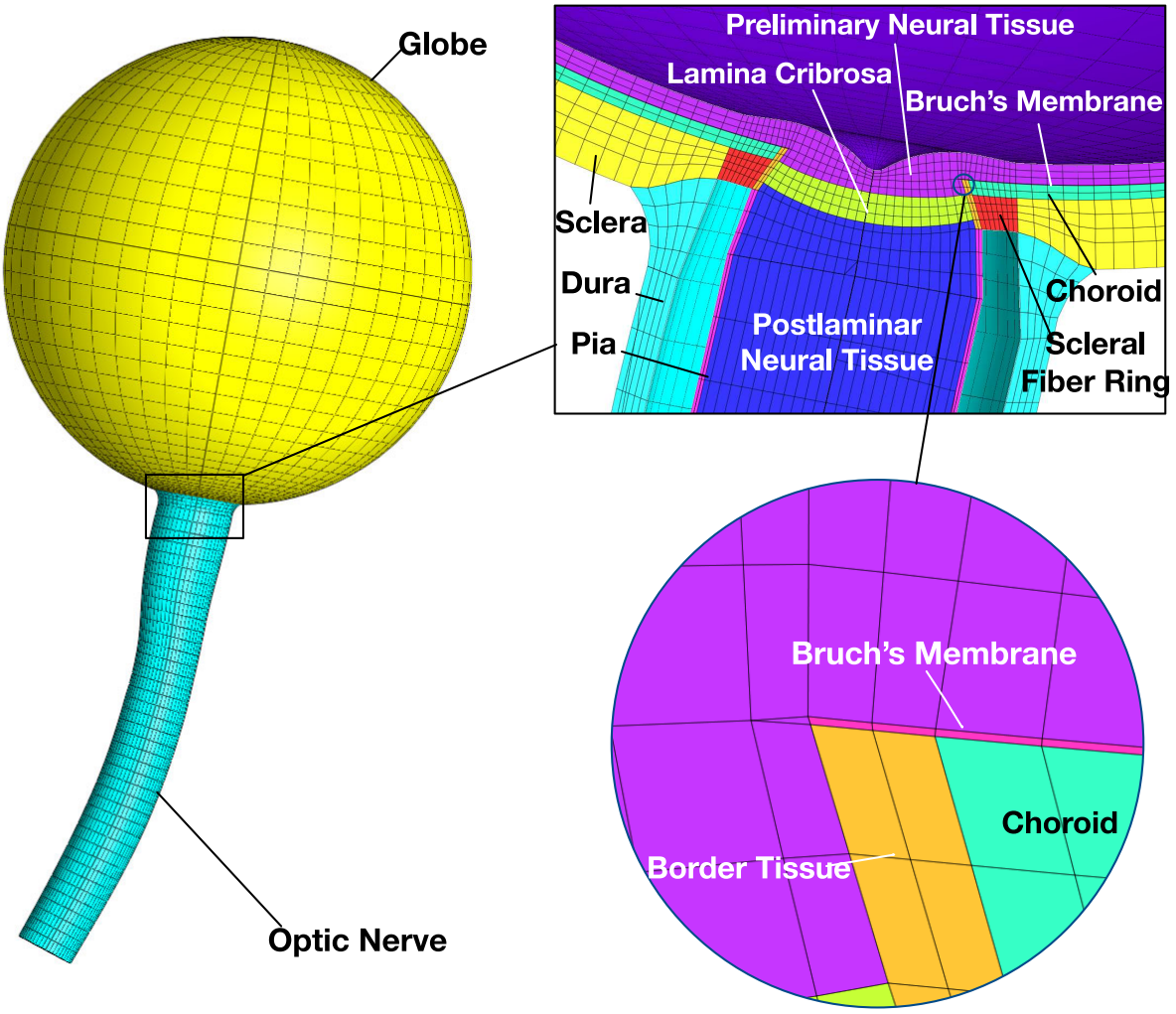

Figure 1. Reconstructed geometry and FE mesh of the whole eye model adopted from Jin et al.[19] ONH structures (including the LC, sclera, neural tissues, choroid, Bruch's membrane, border tissue, pia, and dura) were reconstructed using average measurements from the literature.[9,19,24,26,74]

then subjected to a maximum of 5% strain at a rate of 1% per second, followed by a relaxation period of 300 seconds at constant strain. The total relaxation period was chosen to be 300 seconds, after which stress changes were less significant (less than 1% over 5 seconds). The tensile strain was defined as the ratio of LC elongation to its original length as measured before the test. These strain levels were chosen as they are typically exhibited in vivo under physiological conditions (during eye movements or change in IOP).[10] The thickness measurements of the LC (mean: 0.628 mm) were obtained before each test by spectral-domain OCT (Spectralis OCT, Heidelberg Engineering, Heidelberg, Germany) and were used to compute the tensile stress.

The averaged stress values of seven porcine eyes were fitted with a linear viscoelastic model incorporating a reduced relaxation function as shown in Equation (2) to characterize the viscoelastic properties of the LC.[30] The following discrete relaxation function was employed:

$$G(t) = 1 + \ln\left(\frac{\tau_L}{\tau_S}\right)\frac{c}{n}\sum_{i=1}^{n} e^{-t/\tau_i} \quad (2)$$

where c is the spectral magnitude, τ_S and τ_L are the short-term and long-term relaxation time constants, respectively. In the discrete spectral relaxation function, n is the number of spectral time constants and

$$\tau_i = 10^{[\log(\tau_S)+(i-1)\Delta\tau]} \text{ where } \Delta\tau = \frac{\log(\tau_L) - \log(\tau_S)}{(n-1)} \quad (3)$$

Table 1. Tissue Biomechanical Properties used for all Models

Tissue	Constitutive Model	Biomechanical Properties	References
Sclera	Mooney-Rivlin Von Mises distributed fibers	c1 = 0.285 MPa c3 = 0.0137 MPa c4 = 658.125 kf = 2 (scleral ring) kf = 0 (other region of sclera) θ_p: preferred fiber orientation	Girard et al.[25]
LC	Viscoelastic	$\gamma_1 = 8.148$ $\gamma_2 = 8.148$ $\tau_1 = 8.33$ s $\tau_2 = 272$ s Elastic material: Neo-Hookean Elastic modulus = 0.49 MPa Poisson's ratio = 0.49	Porcine tissue experiment (this study)
Neural tissue	Isotropic elastic	Elastic modulus = 0.03 MPa Poisson's ratio = 0.49	Miller[75]
Bruch's membrane	Isotropic elastic	Elastic modulus = 10.79 MPa Poisson's ratio = 0.49	Chan et al.[76]
Choroid	Biphasic	Solid volume fraction: 0.55 Solid matrix: Neo-Hookean C1 = 0.015 MPa D1 = 0 MPa Permeability: 45,037 mm^2/MPa	Jin et al.[19]
Dura	Yeoh model	C1 = 0.1707 MPa C2 = 4.2109 MPa C3 = –4.9742 MPa	Wang et al.[24]
Pia	Yeoh model	C1 = 0.1707 MPa C2 = 4.2109 MPa C3 = –4.9742 MPa	Wang et al.[24]
Border tissue	Isotropic elastic	Elastic modulus = 10.79 MPa Poisson's ratio = 0.49	Chan et al.[76]

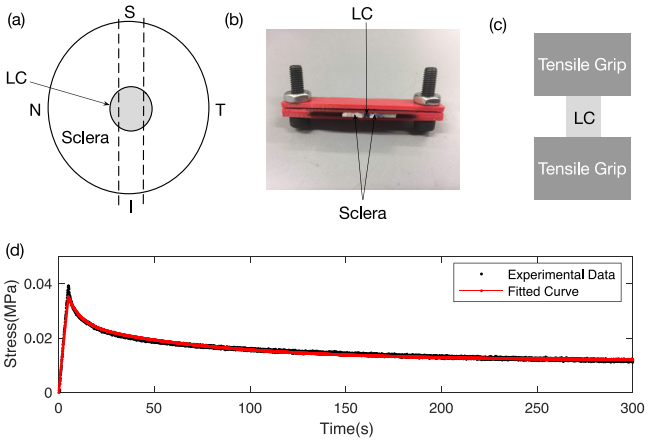

Figure 2. (a) Schematic showing the scleral strip with the LC in its center. The uniaxial tensile specimen was obtained by using a customized device (shown in b) to obtain a fixed width of 1.2 mm. It was then clamped between the tensile grips (shown in c) with the LC exposed in its center. (d) A typical stress relaxation experimental test dataset for an LC sample fitted with a linear viscoelastic model curve.[30]

For a linear increase in strain at a finite rate, the stress response at time t would be expressed as

$$\sigma(t) = \int_0^t G(t-\xi)\frac{\partial \sigma^e(\varepsilon)}{\partial \varepsilon}\frac{\partial \varepsilon}{\partial \xi}d\xi,$$

$$\text{where } \varepsilon(t) = \begin{cases} \dot{\varepsilon}t, & for\ 0 \le t \le t_0 \\ \varepsilon_0, & for\ t_0 \le t \end{cases} \quad (4)$$

where $\dot{\varepsilon}$ represents the strain rate, and $t_0 = 5\,s$. Hence according to Equation (4), the stress response becomes

$$\sigma(t) = \dot{\varepsilon}E_\infty\left\{\ln\left(\frac{\tau_L}{\tau_S}\right)\frac{c}{n}\sum_{i=1}^{n}\tau_i\left(1-e^{-\frac{t}{\tau_i}}\right)+t\right\}$$

$$\text{for } 0 \le t \le t_0 \quad (5)$$

$$\sigma(t) = \dot{\varepsilon}E_\infty\left\{\ln\left(\frac{\tau_L}{\tau_S}\right)\frac{c}{n}\sum_{i=1}^{n}\tau_i(e^{\frac{t_0}{\tau_i}}-1)e^{-\frac{t}{\tau_i}}+t_0\right\}$$

$$\text{for } t_0 \le t \quad (6)$$

Equations (5) and (6) were fitted simultaneously to the tensile ramping and the relaxation phase. A typical stress relaxation curve is shown in Figure 2d. The fitting parameters can be found in Table 2 (mean ± SD).

Table 2. Viscoelastic Material Properties of the LC from the Experiment

Viscoelasticity of the LC	
Instantaneous modulus (E_{0+} *)	8.49 ± 1.02 MPa
Equilibrium modulus (E_∞)	0.49 ± 0.29 MPa
Long-term time constant (τ_L)	272 ± 169 s
Short-term time constant (τ_S)	8.33 ± 1.75 s

* $E_{0+} = [1 + c \ln\left(\frac{\tau_L}{\tau_S}\right)]E_\infty$.

In FEBio v2.8.5 (Musculoskeletal Research Laboratories, University of Utah, Salt Lake City, UT, USA), the linear viscoelastic model was defined in the same manner[33] as shown in Equation (7):

$$S(t) = \int_{-\infty}^{t} G(t-s)\frac{dS^e}{ds}ds, \quad (7)$$

where S^e is the elastic stress and G is the discrete relaxation function. This latter is defined as

$$G(t) = 1 + \sum_{i=1}^{n} \gamma_i e^{-t/\tau_i} \quad (8)$$

where γ_i, τ_i represent the viscoelastic and relaxation time coefficients, respectively. In this model, we chose $n = 2$ and derived the viscoelastic and relaxation time coefficient by comparing relaxation functions from equation (2) and (8). The elastic component was modeled using Neo Hookean elastic material with the elastic modulus the same as the equilibrium modulus. A simulated stress relaxation test was performed in FEBio to verify that the predicted stress value as a function of time agrees with the experimental stress behavior. The detailed input can be found in Table 1.

Boundary and Loading Conditions

Two sets of boundary conditions were applied to ensure numerical stability. First, the orbital apex of the optic nerve was fixed to model its connection to the optic canal. Second, the eye globe was fixed near the equator on two opposite sides with four nodes on each side. This was carried out to improve stability, and as such boundary condition had no impact on the ONH deformations.

We applied a baseline IOP of 15 mm Hg to the inner limiting membrane, and a baseline CSFP of 11.3 mm Hg to the arachnoid space (Fig. 3).[34] As described previously, we applied prescribed fluid pressures on the choroidal layer to mimic the blood flow inlets (long and short posterior ciliary arteries [PCAs]) and outlets [vortex veins]).[19] The arterial pressure was varied between 70.8 and 93 mm Hg to mimic the diastolic and systolic changes of the ophthalmic artery pressure.[35] A constant blood pressure of 15 mm Hg was applied at the four vortex vein exits out of the choroid.[36] In our model, it was the pressure difference between the PCAs and vortex veins that drove the choroidal blood flow, allowing the choroid to swell during the cardiac cycle.

Changing the Heart Rate from 60 to 120 bpm

We aimed to understand the impact of different heart rates on the ocular pulse, ONH deformations, and LC stiffness.

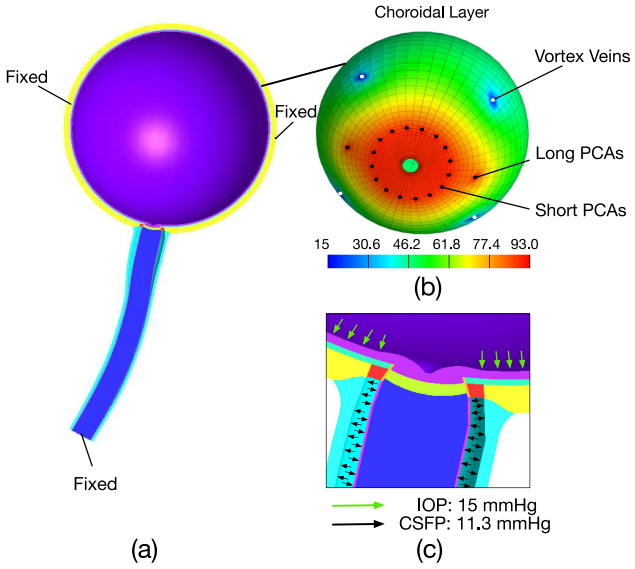

Figure 3. (a) Half eye geometry and boundary conditions: fixed optic nerve at the orbital apex and fixed sclera nodes near the equator on two opposite sides. (b) Choroidal with the nodes in which arterial blood pressure (short and long PCAs) and venous blood pressures (vortex veins) were applied. (c) ONH region illustrating the pressure loads (IOP, CSFP) applied in each model.

Hence four models were implemented with the heart rate ranging from 60 to 120 bpm with an increment of 20 bpm. All the boundary conditions and material properties were kept constant, such that only the heart rate varied.

FE Processing to Predict the OPA, Pulse Volume, and ONH Deformations

All FE models were solved with FEBio.[28] The OPA was estimated by first assuming that the vitreous was incompressible as performed in our previous study.[19] This is a reasonable assumption because the vitreous mostly consists of water, which is also incompressible, and is gas-free. Therefore the volume of the vitreous body was constrained to remain constant during choroidal swelling in all our simulations. Considering that our model aimed to reproduce choroidal swelling during the cardiac cycle, such a swelling will try to deform and change the volume of the vitreous body. Because the vitreous body was constrained as incompressible, an internal pressure needed to be applied to maintain its volume. This pressure term is an output of our model and can be understood as the OPA.

More specifically, each model was implemented in three steps as shown in Figure 4. The initial step applied boundary conditions and loads, including baseline IOP, CSFP, and ophthalmic arterial pressure, and vortex vein pressure. During the second step, a 5000 second relaxation period was applied because of the viscoelasticity of the LC. The 5000 second relaxation period was to provide sufficient relaxation of the viscoelastic LC and prevent interferences between the stress relaxation and pulsatile deformation in the next step. All the boundary conditions and loads remained unchanged. During the final step, we imposed a volume constraint to the inner limiting membrane to ensure the incompressibility of the vitreous.[19] The details of the volume constraint and OPA derivation can be found in our previous article.[19] In

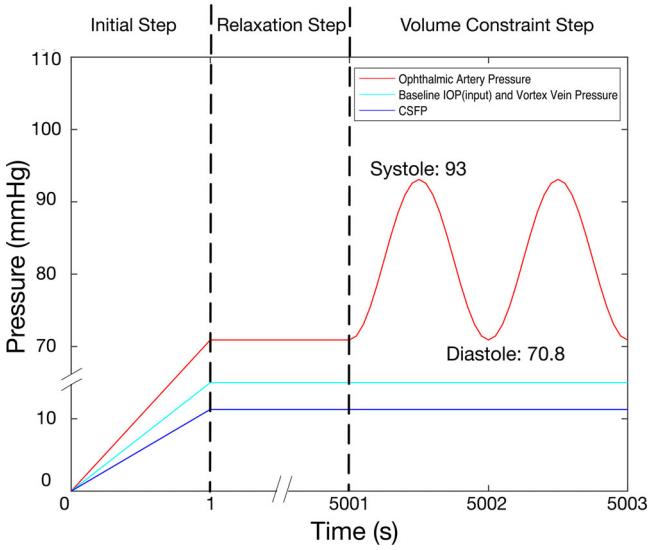

Figure 4. Profiles of different pressure loads.

brief, the volume constraint of the inner limiting membrane is achieved through an augmented Lagrangian approach.

$$p_{k+1} = p_k + \varepsilon * (V - V_0) \quad (9)$$

where p is the fluid pressure, k is the augmentation iteration, ε is a user-defined penalty factor, V and V_0 are the current (i.e., final) and initial volume of the vitreous body, respectively. This pressure is applied to the entire enclosed surface of the constrained volume and it is updated until the current (i.e., final) volume matches the original volume. Hence this pressure represents the pressure change (i.e., the OPA) required to counterbalance the external perturbation (i.e., choroidal expansion) to maintain the volume of the vitreous body. The CSFP, baseline IOP, and vortex vein pressure were kept constant; the ophthalmic arterial pressure varied from diastole to systole periodically following a sinusoidal profile for two cycles. The time step at the pulsation was 0.025 seconds, and a temporal convergence test confirmed that the simulation results did not depend on the time step size; the predicted parameters varied less than 1% with more than 50% change in time step size. A quasistatic simulation was adopted because of the slow frequency (1–2 Hz) and small density of the ocular tissues.

The post-processing was performed using MATLAB v.2018 (MathWorks, Natick, MA, USA). For each model, we reported the OPA, the pulse volume, the diastole-to-systole displacements of the LC, and of the prelamina tissue. In addition, we characterized the stiffness of the LC at different heart rates in the central region along the radial, circumferential, and longitudinal directions (Fig. 5).

Characterizing LC Stiffness with Changing Heart Rate

To understand the dynamic behavior of the LC during the cardiac cycles and in response to the ocular pulse, we characterized the stiffness of the LC from FE modeling results at different heart rates. The stiffness of the LC can be characterized by computing its dynamic modulus, as typically performed for dynamic mechanical analyses.[20] Because the

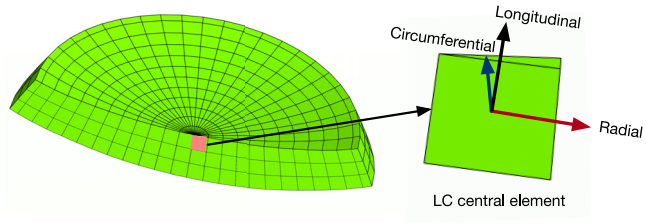

Figure 5. Cross-section of the LC illustrating the local coordinates (radial, circumferential, and longitudinal) for one central element.

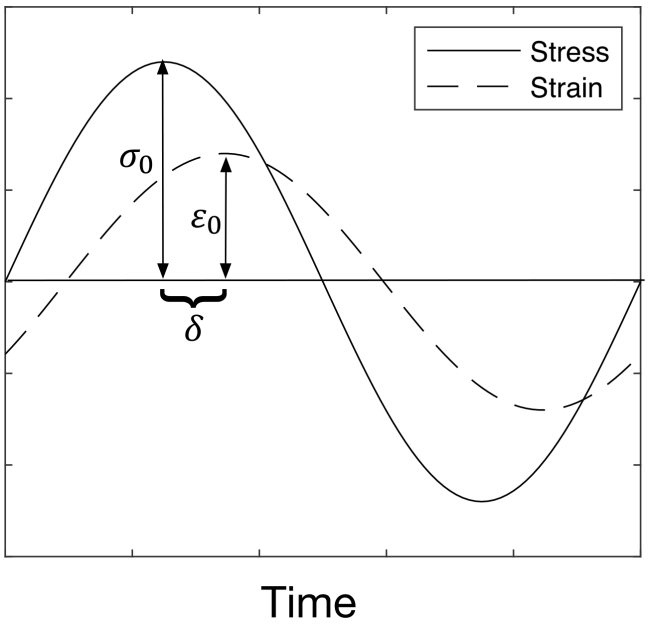

Figure 6. Schematic representation of the strain and stress profiles as a function of time in calculating the dynamic properties of the LC.

ocular pulse induced a cyclic deformation of the LC, the LC strain "input" can be represented as:

$$\varepsilon = \varepsilon_0 \sin(\omega t + \delta_\varepsilon) \quad (10)$$

where ε_0, δ_ε, and ω are the peak strain amplitude, strain phase shift, and angular frequency of the harmonic excitation, respectively. Because the LC only exhibits small strains, the LC can be approximated to be linear viscoelastic.[37] Hence the resulting sinusoidal stress "output" would differ in phase from the "input" strain depending on the viscoelastic properties of the LC, and can be expressed as:

$$\sigma = \sigma_0 \sin(\omega t + \delta_\sigma) \quad (11)$$

where σ_0 and δ_σ are the peak stress amplitude and stress phase shift, respectively. The phase delay between the stress and the strain due to viscoelastic effects is known as the phase lag δ, that is, the difference between δ_ε and δ_σ (Fig. 6). The dynamic mechanical properties of the LC can now be represented by the complex dynamic modulus, consisting of the storage modulus (elastic component) and

Investigative Ophthalmology & Visual Science

the loss modulus (viscous component). It is defined as:

$$E^* = \frac{\sigma}{\varepsilon} = E' + iE'' \quad (12)$$

where E' is the storage modulus, E'' is the loss modulus, and i the unit imaginary number. The storage and loss moduli are related to the phase lag through the following equations:

$$E' = E * \cos(\delta), \quad (13a)$$

$$E'' = E * \sin(\delta) \quad (13b)$$

For each heart rate, we computed the storage and loss moduli in the central region of the LC (composed of one element) as shown in Figure 5. We first computed the Lagrange strain and Cauchy stress tensors and estimated the diastole-to-systole Lagrange strain and Cauchy stress profiles along three directions (radial, circumferential, and longitudinal). Each strain/stress profile was then fitted with Equations (10–11) to determine the peak strain/stress amplitudes and the phase shifts. From these data we extracted the phase lag, and thus the storage and loss moduli of the LC central region along three directions: radial, circumferential, and longitudinal.

Results

Effect of the Heart Rate on the Ocular Pulse

For each model, the pulsating arterial pressure during the cardiac cycle resulted in choroidal swelling (increase in pulse volume), which in turn increased the IOP (the delta change in IOP being the OPA). The IOP and the pulse volume as functions of time are shown in Figure 7 for two cycles at a heart rate of 60 bpm.

We also found that both the OPA and the pulse volume decreased with an increasing heart rate (Fig. 7). On average, the OPA and the pulse volume decreased by 0.04 mm Hg (2.7%) and 0.13 µL (2.8%), respectively, for every 10 bpm heart rate increment.

Effect of the Heart Rate on ONH Deformations

During the cardiac cycle, the ONH moved posteriorly (diastole to systole) and anteriorly (systole to diastole). The diastole to systole displacement of the central anterior LC point was 5.8 µm at a heart rate of 60 bpm, and decreased by 0.1 µm for every 10 bpm heart rate increment (Figs. 8a–c).

We also observed that the prelamina (neural tissue anterior to the lamina) and the parapapillary retina moved along opposite directions during the cardiac cycle. Specifically, from diastole to systole, the prelamina moved posteriorly (as highlighted in red in Fig. 8d), whereas the parapapillary retina (highlighted in black in Fig. 8d) moved anteriorly. This resulted in a net shearing of the neural tissues in the neuroretinal rim. This shearing amount (difference between the prelamina displacement and the parapapillary retina displacement) also decreased with an increasing heart rate. On average, the shearing amount reduced by 0.12 µm for every 10 bpm heart rate increment (Fig. 8f).

Effect of the Heart Rate on LC stiffness

The storage and loss moduli were computed in the central region of the LC for three orientations (radial, circumferential, and longitudinal). They all followed the exact same trend, and all increased with an increasing heart rate (Fig. 9). On average, the storage modulus increased by 0.014 MPa, and the loss modulus by 0.04 MPa for every 10 bpm heart rate increment. This indicates that the LC will appear stiffer with a higher heart rate.

Discussion

In this study, we used FE modeling to study the impact of the heart rate on the ocular pulse and its biomechanical impact on the ONH. Our model predicted that the OPA, pulse volume, and ONH deformations decreased with an increasing heart rate. In addition, the LC became stiffer at faster heart rates. These findings may help develop technologies to finely assess the biomechanical properties of the ONH in vivo.

The OPA and the Pulse Volume Decreased with an Increasing Heart Rate

With an increase in heart rate, both the OPA and the pulse volume reduced when simultaneously the ophthalmic arterial and venous vein pressures were kept constant. A faster heart rate is associated with a shorter duration for each cardiac cycle, suggesting that the volume of blood being pushed into the choroid would be reduced for each pulse. Our results are also consistent with a previous clinical study,[23] in which all the subjects were fitted with cardiac pacemakers and the heart rate was altered by resetting the pacemakers. Neither IOP nor systolic-diastolic blood pressures were found to be significantly altered during the experiments, suggesting that the heart rate was one of the main contributing factors causing a reduction in OPA. In the Trew et al.[23] study, the OPA decreased by 0.12 mm Hg (7.4%) for every 10 bpm heart rate increment, which was higher in magnitude than our predicted results (0.04 mm Hg, 2.7%). This difference could potentially be attributed to the variations in the material properties and morphologies between the patients and our models.

Note that the change in OPA with heart rates varying from 60 to 120 bpm was approximately 16.2%, which was smaller compared with variations in other factors, including IOP, scleral stiffness, and ophthalmic artery pressures. Our previous work predicted a 35.7% increase in OPA with IOP changing from 15 to 30 mm Hg.[19] Also, with a 20% increase in scleral stiffness and ophthalmic artery pressures, OPA increased by 22% and 22.5%, respectively. Although the impact of the heart rate on OPA was smaller compared with other parameters, it is still an important factor to study because it has a short-term impact and is affected by common activities, such as exercise. It has also been observed that a short period of dynamic exercise can also lead to a reduction in OPA and ocular pulse volume.[38–40] However, the impact of exercise is complex as it involves changes in multiple physical parameters including not only the IOP and heart rate, but also the systolic and diastolic blood pressures, and blood distribution in the body. Although heart rate and blood pressures involve separate mechanisms, exercise would induce an increase in both heart rate and blood pressures.[41] The systolic and diastolic blood pressures are related to the ocular pulse through the ocular perfusion pressure (OPP), defined as the difference between the mean blood pressure and IOP. In one study, there was a significant reduction in IOP, and an

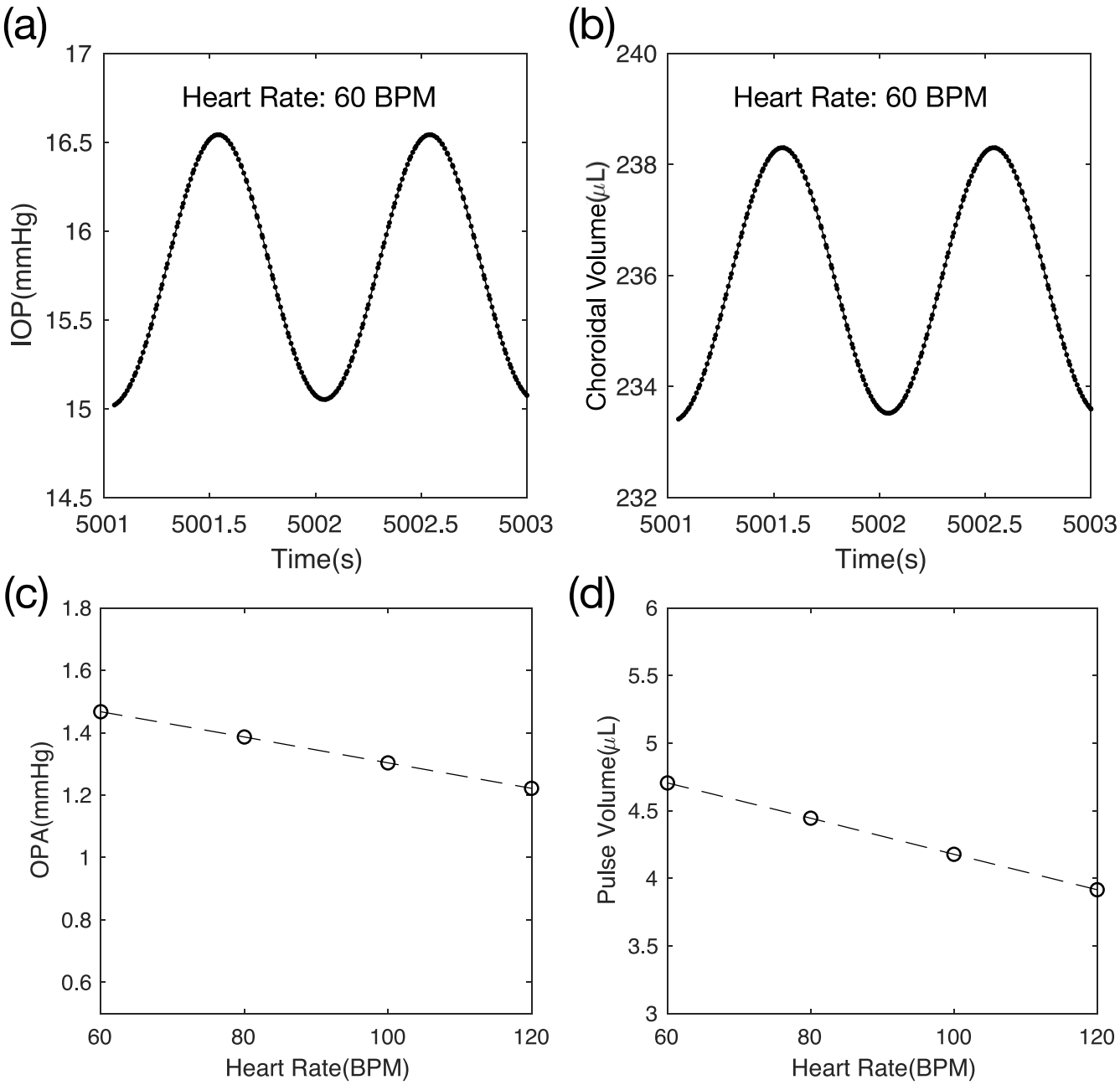

Figure 7. (a,b) IOP and choroidal volume over two cycles at a heart rate of 60 bpm. (c,d) Change of the OPA and the pulse volume with heart rate.

increase in OPP immediately after strenuous exercise (resting: heart rate = 68 ± 7.9 bpm, IOP = 19.8 ± 5.4 mm Hg, OPP = 51.2 ± 4.9 mm Hg; after exercise: heart rate = 125 ± 24.9 bpm, IOP = 14.3 ± 5.0 mm Hg, OPP = 56.9 ± 7.5 mm Hg).[40] Our models could potentially be used to reproduce more complex scenarios such as those.

ONH Deformations and Neural Tissue Shear Decreased with an Increasing Heart Rate

Our model predicted that ONH deformations decreased with an increasing heart rate. It has been shown that isometric exercise caused a significant increase in the mean arterial blood pressure and pulse rate, and decreased the fundus pulsation amplitude, as measured by laser interferometry.[22] Despite changes in the mean arterial blood pressure, reduced fundus pulsation amplitude may indicate a decrease in ONH deformations at a faster heart rate, which is consistent with our predicted results.

From diastole to systole, the shearing amount refers to the anterior movement of the parapapillary retina because of the choroidal expansion and the posterior ONH deformation due to both choroidal swelling and the OPA. With an increase in heart rate, it is expected that the shearing amount would decrease because of the reduced OPA and pulse volume. This shearing phenomenon has been observed in vivo in humans using low-coherence tissue interferometry.[18]

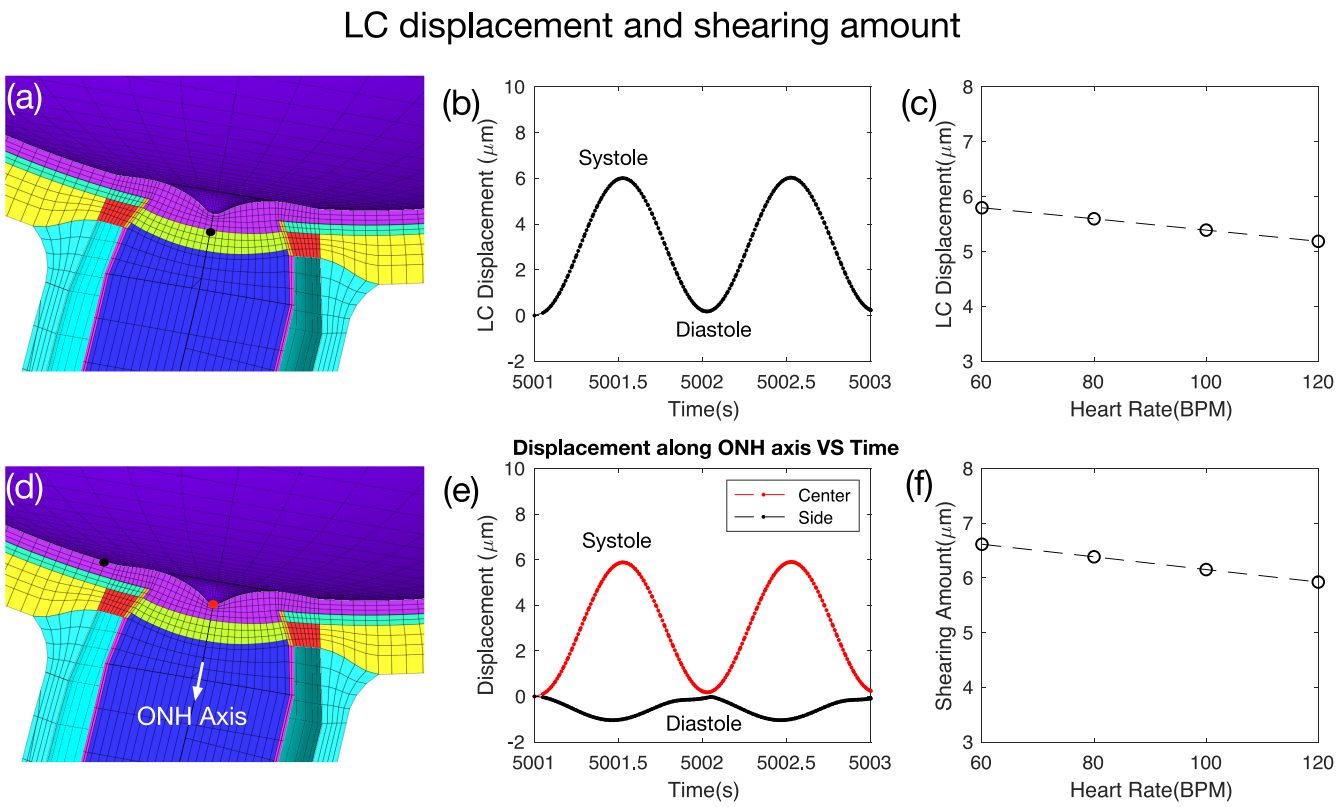

Figure 8. (a) Cross-section of the ONH highlighting the center of the LC, and (b) the displacement of the LC center. (c) Change of the LC displacement with increasing heart rate. (d,e) Cross-section of the ONH and the radial displacement of the highlighted points (red: center of prelaminar; black: a point on the retinal surface located 0.65 mm away from Bruch's membrane opening (BMO)) over two cardiac cycles. (f) Change of the shearing amount with heart rate.

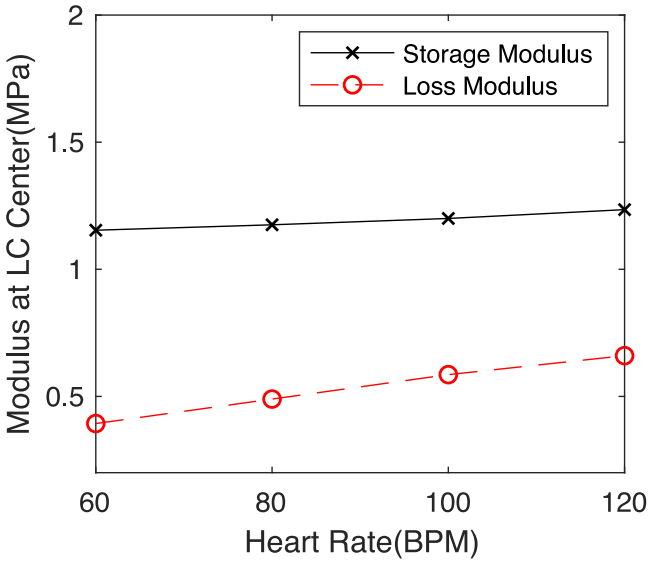

Figure 9. Change of the storage and loss moduli of the LC center with the heart rate.

The LC Became Stiffer with an Increasing Heart Rate

Our model predicted that the dynamic modulus of LC increased with an increasing heart rate. Similar phenomena have also been observed in other viscoelastic biological tissues, such as the cornea[42,43] intervertebral discs,[44] and other biomaterials.[45] The dynamic modulus characterizes the stiffness of a material in response to dynamic loading, and it can differ from its static behavior because viscoelastic materials typically become more rigid with a faster loading rate.[42,43] The static modulus describes the elasticity of a tissue at "equilibrium," whereas the dynamic modulus provides information about the instant stiffness of a material. For instance, for the cornea, the dynamic properties are likely dominated by the rearrangement of the extracellular matrix (mainly through diffusion of water) on changes in stress, whereas the static properties are more closely related to the collagen structure.[46] Histological studies have shown that the morphology of the LC, as a porous, reticulated, and multilamellar sieve-like structure, mainly comprises of laminar beams consisting of elastin fibers and collagen fibrils (types I and III).[47] Hence it is likely that the dynamic and static responses of the LC are also dominated by different components, and both may change differently during the progression and development of glaucoma.

Clinical Relevance to Glaucoma Pathogenesis

At first view, a faster heart rate may be beneficial for the eye. First, it resulted in a smaller OPA, and hence smaller ONH deformations. A larger deformation would yield larger stain/stress fluctuations within the LC, which may have an impact on the RGC axons and the vascular capillaries. This is also consistent with the fact that a larger OPA has been

observed in chronic angle-closure glaucoma and suspected open-angle glaucoma subjects.[48]

Second, a faster heart rate also resulted in lower neural tissue shear, which may limit axonal damage in the neuroretinal rim region.[49–51] As discussed in our previous work, repeated shearing of axons in the neuroretinal rim region could potentially contribute to axonal damage. The neuroretinal rim is indeed a region that exhibits a mechanical discontinuity: it is where RGC axons follow a sharp turn to enter the disc. In this region, a reduction in Bruch's-membrane-opening minimum-rim-width has been observed clinically in glaucoma and in elderly individuals.[49–54] Hence decreasing shearing with a faster heart rate may be seen as "mechanically protective."

Third, the LC was found to stiffen with an increasing heart rate, which could provide better support to the RGCs and vasculatures. Pseudoexfoliation (PEX) syndrome is a systemic disorder of the elastic fiber system, which can lead to PEX glaucoma. It has been reported that the stiffness of the LC in PEX eyes is 40% less than that in normal eyes as evaluated by atomic force microscopy.[55] This decrease in LC stiffness may increase susceptibility to IOP-induced glaucomatous optic nerve damage as observed in PEX eyes, and thus dynamic stiffening of the LC may also be seen as beneficial.

However, the situation may be more complex as the effects of dynamic loading at the cellular level has remained elusive yet. The response of cells to deformation is dependent on both the magnitude and the rate of mechanical strain. Some studies have shown that short-term strain or stress variations can lead to cellular injury in neurons and neuron-like cells.[56–58] Future research is required to better understand the link between dynamic loading and RGC axonal injury at the micro or cellular scale.

Understanding the Clinical Implications of LC Stiffening

During the development and progression of glaucoma, the connective tissues of the ONH undergo constant remodeling (including stiffening in the moderate/severe stages) and extensive structural changes.[59] The extracellular matrix remodeling are usually characterized by fibrotic changes associated with cellular and molecular events, such as myofibroblast activation, that could drive further tissue fibrosis and stiffening.[60] However, as discussed herein, the LC also gets stiffer with an increased heart rate. Ex vivo strain measurement shows that the stiffness of the LC increases with age.[61] It is believed that the change in LC stiffness because of the change in heart rate and aging involves different mechanisms. Our results only reflect the short-term impact of a raised heart rate, and we do not know whether the stiffening of the lamina will become chronic or whether other homeostatic mechanisms might reverse these changes in the longer term. If an increase in dynamic LC stiffness is proved to be beneficial, it is possible to modulate heart rate in the longer term via pharmacologic means. Finally, it is important to note that while assessing the material properties of the LC from the ocular pulse, physicians should be able to distinguish whether a change in LC stiffness is because of a different heart rate/blood pressure, or because of tissue remodeling. This information may be helpful to predict glaucoma progression.

Limitations

Our study has several limitations. First, our model did not consider the regional variations in the scleral thickness and stiffness, which are known to exist in monkeys, canines, and humans.[20,62,63] The regional variations may affect the prediction of the OPA.

Second, the choroid was simplified and modeled as a biphasic material, consisting of a porous solid phase (connective tissues) and a fluid phase (blood). In addition, the permeability of the choroid was approximated grossly from the vascular resistance, the average diameter of the choroid, and the blood viscosity.[19] The complex microvasculature architecture, as well as the blood flow of the choroid, cannot be fully captured by this description. For instance, the segmental distribution of PCAs[64] and the autoregulatory capacity of the choroid[22,65] were not considered in our model. Furthermore, the PCAs and vortex veins were not modeled explicitly but represented by prescribed fluid pressures. Future work may need to assess the permeability of the choroid experimentally and also consider more complex material models to better describe the behavior of the pulsatile choroidal blood flow.

Third, our model did not account for the blood circulation within the LC and other pulsatile components, including those from the retina, central retinal artery, and the CSFP. These pulsations may affect the LC deformations as well. The pulsation of the CSFP is phase-shifted with respect to the ocular pulse, such that the CSFP peak occurs slightly before that of the IOP.[66,67] The phase difference between the IOP and CSFP may lead to dynamic fluctuations of the translaminar pressure gradient, resulting in different ONH deformation profiles. The contribution of these pulsatile components may be important and should be considered in future studies.

Fourth, the geometry of the eye was constructed from a single eye model, and the dimensions of the ONH were taken as average measurements from the literature. However, the ocular and ONH geometries can vary widely across individuals, and thus may influence the predicted ocular pulse significantly. In our model, the retina, choroid, and Bruch's membrane were simplified as a uniform layer throughout the eye. We aim to take regional variations in tissue thickness into consideration in future work.

Fifth, we experimentally measured the viscoelastic material properties of the porcine LC through a uniaxial stress relaxation test. The aspect ratio (2:1) of the LC sample was small and it may induce edge or clamping effects. During such a test, the LC may exhibit a stress softening effect (Mullins effect) that depends on the maximum load that it was subjected to during its loading history.[68] The strain level (5%) at stress relaxation stage exceeded the strain amplitude (1%) at the preconditioning cycles. Although the stress relaxation performed at 5% strain did not involve repeated loading and unloading processes, the viscoelastic material properties identified were likely affected by the stress softening effect. In addition, the LC was simplified as a homogeneous material, and we used a simple test to assess its properties; under physiological conditions, the LC is not just simply loaded uniaxially. The complicated laminar microarchitecture was not considered. Microlevel modeling of the laminar beams predicted higher strain and stress than those predicted by macroscale models of the ONH.[69] The mean strain of the laminar beams varies greatly across different nonhuman primates and depends on the three-dimensional

geometry of each eye's ONH connective tissues.[69,70] Models incorporating the microlevel laminar beams may be considered in the future.

Sixth, for simplicity and as a first approach, we only modeled the viscoelasticity of the LC and not that of other tissues, such as the choroid and the sclera. We focused on the LC only as it is a tissue that has been observed under dynamic loading[18] and because it plays a critical role in glaucoma as the main site of damage. The time-dependent LC was assumed to be ideally bonded to the rest of tissues (time-independent). This was implemented through enforcing that the two materials at the interface shared the same nodes. More complex models will be needed in the future to better understand how scleral and choroidal viscoelasticity could interact with the LC.

Seventh, the results shown only reflect the short-term impact of a raised vheart rate, and we do not know whether the stiffening of the lamina will become chronic or whether other homeostatic mechanisms might reverse these changes in the longer term.

Eighth, the LC was modeled as a uniform and isotropic structure. We did not consider potential differences in the anatomy and biomechanical properties of the various layers of the LC, nor did we consider lateral movements of the LC in dependence of changes of the examined parameters, and in dependence of the obliqueness of the optic nerve canal, and the spatial relationship between Bruch's membrane opening and the LC position.[71,72] In addition, the storage and loss moduli were only characterized in the central region of the LC, but they actually varied regionally (see Supplementary material). In our study, the central region of the LC was chosen for consistent comparison of the dynamic moduli at different heart rates.

Ninth, the aqueous humor secretion and outflow facility of the anterior chamber were not included in our model. Because the outflow facility directly control the baseline IOP,[73] this may also have an impact on the OPA. Future studies may consider more realistic anterior chamber geometries while taking the aqueous humor flow into consideration.

Conclusions

In this study, we used FE modeling to study the ocular pulse and the impact of the heart rate on ONH deformations. We found that the OPA, the pulse volume, and the ONH deformation reduce at a faster heart rate. Our models also indicated that the LC becomes stiffer with increasing heart rate. These results will help us develop technology to assess the biomechanics of the ONH in vivo by using the ocular pulse as a natural load.

Acknowledgments

Supported by the Singapore Ministry of Education, Academic Research Fund, Tier 2 (R-397-000-280-112).

Disclosure: **Y. Jin**, None; **X. Wang**, None; **S.F.R. Irnadiastputri**, None; **R.E. Mohan**, None; **T. Aung**, None; **S.A. Perera**, None; **C. Boote**, None; **J.B. Jonas**, None; **L. Schmetterer**, None; **M.J.A. Girard**, None

References

1. Abegão Pinto L, Willekens K, Van Keer K, et al. Ocular blood flow in glaucoma–the Leuven Eye Study. *Acta Ophthalmol*. 2016;94:592–598.
2. Coudrillier B, Tian J, Alexander S, Myers KM, Quigley HA, Nguyen TD. Biomechanics of the human posterior sclera: age- and glaucoma-related changes measured using inflation testing. *Invest Ophthalmol Vis Sci*. 2012;53:1714–1728.
3. Ethier CR. Scleral biomechanics and glaucoma—a connection? *Can J Ophthalmol*. 2006;41:9–14.
4. Girard MJ, Strouthidis NG, Desjardins A, Mari JM, Ethier CR. In vivo optic nerve head biomechanics: performance testing of a three-dimensional tracking algorithm. *J R Soc Interface*. 2013;10:20130459.
5. Burgoyne CF, Downs JC, Bellezza AJ, Suh JK, Hart RT. The optic nerve head as a biomechanical structure: a new paradigm for understanding the role of IOP-related stress and strain in the pathophysiology of glaucomatous optic nerve head damage. *Prog Retin Eye Res*. 2005;24:39–73.
6. Downs JC. Optic nerve head biomechanics in aging and disease. *Exp Eye Res*. 2015;133:19–29.
7. Downs JC, Roberts MD, Burgoyne CF. The mechanical environment of the optic nerve head in glaucoma. *Optom Vis Sci*. 2008;85:425–435.
8. Girard MJ, Suh JK, Bottlang M, Burgoyne CF, Downs JC. Biomechanical changes in the sclera of monkey eyes exposed to chronic IOP elevations. *Invest Ophthalmol Vis Sci*. 2011;52:5656–5669.
9. Sigal IA, Flanagan JG, Tertinegg I, Ethier CR. Predicted extension, compression and shearing of optic nerve head tissues. *Exp Eye Res*. 2007;85:312–322.
10. Wang X, Beotra MR, Tun TA, et al. In vivo 3-dimensional strain mapping confirms large optic nerve head deformations following horizontal eye movements. *Invest Ophthalmol Vis Sci*. 2016;57:5825–5833.
11. Jonas JB, Wang N, Yang D, Ritch R, Panda-Jonas S. Facts and myths of cerebrospinal fluid pressure for the physiology of the eye. *Prog Retin Eye Res*. 2015;46:67–83.
12. Wang X, Fisher LK, Milea D, Jonas JB, Girard MJ. Predictions of optic nerve traction forces and peripapillary tissue stresses following horizontal eye movements. *Invest Ophthalmol Vis Sci*. 2017;58:2044–2053.
13. Girard MJ, Beotra MR, Chin KS, et al. In vivo 3-dimensional strain mapping of the optic nerve head following intraocular pressure lowering by trabeculectomy. *Ophthalmology*. 2016;123:1190–1200.
14. Agoumi Y, Sharpe GP, Hutchison DM, Nicolela MT, Artes PH, Chauhan BC. Laminar and prelaminar tissue displacement during intraocular pressure elevation in glaucoma patients and healthy controls. *Ophthalmology*. 2011;118:52–59.
15. Fazio MA, Johnstone JK, Smith B, Wang L, Girkin CA. Displacement of the lamina cribrosa in response to acute intraocular pressure elevation in normal individuals of African and European Descent. *Invest Ophthalmol Vis Sci*. 2016;57:3331–3339.
16. Girard MJ, Tun TA, Husain R, et al. Lamina cribrosa visibility using optical coherence tomography: comparison of devices and effects of image enhancement techniques. *Invest Ophthalmol Vis Sci*. 2015;56:865–874.
17. Motschmann M, Muller C, Kuchenbecker J, et al. Ophthalmodynamometry: a reliable method for measuring intracranial pressure. *Strabismus*. 2001;9:13–16.
18. Dragostinoff N, Werkmeister RM, Klaizer J, Groschl M, Schmetterer L. Time course and topographic distribution of ocular fundus pulsation measured by low-coherence tissue interferometry. *J Biomed Opt*. 2013;18:121502.
19. Jin Y, Wang X, Zhang L, et al. Modeling the origin of the ocular pulse and its impact on the optic nerve head modeling the origin of the ocular pulse. *Invest Ophthalmol Vis Sci*. 2018;59:3997–4010.

20. Palko JR, Pan X, Liu J. Dynamic testing of regional viscoelastic behavior of canine sclera. *Exp Eye Res*. 2011;93:825–832.
21. Pavlatos E, Ma Y, Clayson K, Pan X, Liu J. Regional deformation of the optic nerve head and peripapillary sclera during IOP elevation. *Invest Ophthalmol Vis Sci*. 2018;59:3779–3788.
22. Kiss B, Dallinger S, Polak K, Findl O, Eichler HG, Schmetterer L. Ocular hemodynamics during isometric exercise. *Microvasc Res*. 2001;61:1–13.
23. Trew DR, James CB, Thomas SHL, Sutton R, Smith SE. Factors influencing the ocular pulse–the heart rate. *Graefes Arch Clin Exp Ophthalmol*. 1991;229:553–556.
24. Wang X, Rumpel H, Lim WE, et al. Finite element analysis predicts large optic nerve head strains during horizontal eye movements. *Invest Ophthalmol Vis Sci*. 2016;57:2452–2462.
25. Girard MJ, Suh JK, Bottlang M, Burgoyne CF, Downs JC. Scleral biomechanics in the aging monkey eye. *Invest Ophthalmol Vis Sci*. 2009;50:5226–5237.
26. Sigal IA, Flanagan JG, Ethier CR. Factors influencing optic nerve head biomechanics. *Invest Ophthalmol Vis Sci*. 2005;46:4189–4199.
27. Bonet J, Wood RD. *Nonlinear Continuum Mechanics for Finite Element Analysis*. Cambridge, UK: Cambridge University Press; 1997.
28. Maas SA, Ellis BJ, Ateshian GA, Weiss JA. FEBio: finite elements for biomechanics. *J Biomech Eng*. 2012;134:11005.
29. Downs JC, Suh JK, Thomas KA, Bellezza AJ, Hart RT, Burgoyne CF. Viscoelastic material properties of the peripapillary sclera in normal and early-glaucoma monkey eyes. *Invest Ophthalmol Vis Sci*. 2005;46:540–546.
30. Downs JC, Suh JK, Thomas KA, Bellezza AJ, Burgoyne CF, Hart RT. Viscoelastic characterization of peripapillary sclera: material properties by quadrant in rabbit and monkey eyes. *J Biomech Eng*. 2003;125:124–131.
31. Shin A, Park J, Demer JL. Opto-mechanical characterization of sclera by polarization sensitive optical coherence tomography. *J Biomech*. 2018;72:173–179.
32. Carew E, Patel J, Garg A, Houghtaling P, Blackstone E, Vesely I. Effect of specimen size and aspect ratio on the tensile properties of porcine aortic valve tissues. *Ann Biomed Eng*. 2003;31:526–535.
33. Puso M, Weiss J. Finite element implementation of anisotropic quasi-linear viscoelasticity using a discrete spectrum approximation. *J Biomech Eng*. 1998;120:62–70.
34. Linden C, Qvarlander S, Johannesson G, et al. Normal-tension glaucoma has normal intracranial pressure: a prospective study of intracranial pressure and intraocular pressure in different body positions. *Ophthalmology*. 2018;125:361–368.
35. Hayreh SS, Edwards J. Ophthalmic arterial and venous pressures. Effects of acute intracranial hypertension. *Br J Ophthalmol*. 1971;55:649–663.
36. Ethier CR, Johnson M, Ruberti J. Ocular biomechanics and biotransport. *Ann Rev Biomed Eng*. 2004;6:249–273.
37. Fung YC. *Biomechanics: Mechanical Properties of Living Tissues*. New York:Springer; 2013.
38. Read S, Collins M. The short-term influence of exercise on axial length and intraocular pressure. *Eye*. 2011;25:767.
39. Lovasik JV, Kergoat H. Consequences of an increase in the ocular perfusion pressure on the pulsatile ocular blood flow. *Optom Vis Sci*. 2004;81:692–698.
40. Price EL, Gray LS, Humphries L, Zweig C, Button NF. Effect of exercise on intraocular pressure and pulsatile ocular blood flow in a young normal population. *Optom Vis Sci*. 2003;80:460–466.
41. Miyai N, Arita M, Miyashita K, Morioka I, Shiraishi T, Nishio I. Blood pressure response to heart rate during exercise test and risk of future hypertension. *Hypertension*. 2002;39:761–766.
42. Boyce B, Jones R, Nguyen T, Grazier J. Stress-controlled viscoelastic tensile response of bovine cornea. *J Biomech*. 2007;40:2367–2376.
43. Elsheikh A, Wang D, Brown M, Rama P, Campanelli M, Pye D. Assessment of corneal biomechanical properties and their variation with age. *Curr Eye Res*. 2007;32:11–19.
44. Race A, Broom ND, Robertson P. Effect of loading rate and hydration on the mechanical properties of the disc. *Spine*. 2000;25:662–669.
45. Tirella A, Mattei G, Ahluwalia A. Strain rate viscoelastic analysis of soft and highly hydrated biomaterials. *J Biomed Mater Res A*. 2014;102:3352–3360.
46. Kling S, Bekesi N, Dorronsoro C, Pascual D, Marcos S. Corneal viscoelastic properties from finite-element analysis of in vivo air-puff deformation. *PLoS One*. 2014;9:e104904.
47. Tan NY, Koh V, Girard MJ, Cheng CY. Imaging of the lamina cribrosa and its role in glaucoma: a review. *Clin Exp Ophthalmol*. 2018;46:177–188.
48. Cheng L, Ding Y, Duan X, Wu Z. Ocular pulse amplitude in different types of glaucoma using dynamic contour tonometry: diagnosis and follow-up of glaucoma. *Exp Ther Med*. 2017;14:4148–4152.
49. Chauhan BC, Danthurebandara VM, Sharpe GP, et al. Bruch's membrane opening minimum rim width and retinal nerve fiber layer thickness in a normal white population: a multicenter study. *Ophthalmology*. 2015;122:1786–1794.
50. Chauhan BC, O'Leary N, Almobarak FA, et al. Enhanced detection of open-angle glaucoma with an anatomically accurate optical coherence tomography-derived neuroretinal rim parameter. *Ophthalmology*. 2013;120:535–543.
51. Tun TA, Sun CH, Baskaran M, et al. Determinants of optical coherence tomography-derived minimum neuroretinal rim width in a normal Chinese population. *Invest Ophthalmol Vis Sci*. 2015;56:3337–3344.
52. Gmeiner JM, Schrems WA, Mardin CY, Laemmer R, Kruse FE, Schrems-Hoesl LM. Comparison of Bruch's membrane opening minimum rim width and peripapillary retinal nerve fiber layer thickness in early glaucoma assessment. *Invest Ophthalmol Vis Sci*. 2016;57:OCT575–OCT584.
53. Danthurebandara VM, Sharpe GP, Hutchison DM, et al. Enhanced structure–function relationship in glaucoma with an anatomically and geometrically accurate neuroretinal rim measurement. *Invest Ophthalmol Vis Sci*. 2015;56:98–105.
54. Fortune B, Yang H, Strouthidis NG, et al. The effect of acute intraocular pressure elevation on peripapillary retinal thickness, retinal nerve fiber layer thickness, and retardance. *Invest Ophthalmol Vis Sci*. 2009;50:4719–4726.
55. Braunsmann C, Hammer CM, Rheinlaender J, Kruse FE, Schäffer TE, Schlötzer-Schrehardt U. Evaluation of lamina cribrosa and peripapillary sclera stiffness in pseudoexfoliation and normal eyes by atomic force microscopy. *Invest Ophthalmol Vis Sci*. 2012;53:2960–2967.
56. Wostyn P, De Groot V, Audenaert K, De Deyn PP. Are intracranial pressure fluctuations important in glaucoma? *Med Hypotheses*. 2011;77:598–600.
57. McMonnies CW. The interaction between intracranial pressure, intraocular pressure and lamina cribrosal compression in glaucoma. *Clin Exp Optom*. 2016;99:219–226.
58. Edwards ME, Wang SS, Good TA. Role of viscoelastic properties of differentiated SH-SY5Y human neuroblastoma cells in cyclic shear stress injury. *Biotechnol Prog*. 2001;17:760–767.
59. Grytz R, Girkin CA, Libertiaux V, Downs JC. Perspectives on biomechanical growth and remodeling mechanisms in glaucoma. *Mech Res Commun*. 2012;42:92–106.

Investigative Ophthalmology & Visual Science

60. Liu B, McNally S, Kilpatrick JI, Jarvis SP, O'Brien CJ. Aging and ocular tissue stiffness in glaucoma. *Surv Ophthalmol*. 2018;63:56–74.
61. Albon J, Purslow PP, Karwatowski WS, Easty DL. Age related compliance of the lamina cribrosa in human eyes. *Br J Ophthalmol*. 2000;84:318–323.
62. Coudrillier B, Boote C, Quigley HA, Nguyen TD. Scleral anisotropy and its effects on the mechanical response of the optic nerve head. *Biomech Model Mechanobiol*. 2013;12:941–963.
63. Coudrillier B, Campbell IC, Read AT, et al. Effects of peripapillary scleral stiffening on the deformation of the lamina cribrosa. *Invest Ophthalmol Vis Sci*. 2016;57:2666–2677.
64. Hayreh SS. Posterior ciliary artery circulation in health and disease: the Weisenfeld lecture. *Invest Ophthalmol Vis Sci*. 2004;45:749–757; 748.
65. Polska E, Simader C, Weigert G, et al. Regulation of choroidal blood flow during combined changes in intraocular pressure and arterial blood pressure. *Invest Ophthalmol Vis Sci*. 2007;48:3768–3774.
66. Morgan WH, Hazelton ML, Yu D-Y. Retinal venous pulsation: expanding our understanding and use of this enigmatic phenomenon. *Prog Retin Eye Res*. 2016;55:82–107.
67. Morgan WH, Lind CRP, Kain S, Fatehee N, Bala A, Yu D-Y. Retinal vein pulsation is in phase with intracranial pressure and not intraocular pressure. *Invest Ophthalmol Vis Sci*. 2012;53:4676–4681.
68. Lokshin O, Lanir Y. Viscoelasticity and preconditioning of rat skin under uniaxial stretch: microstructural constitutive characterization. *J Biomech Eng*. 2009;131:031009.
69. Roberts MD, Grau V, Grimm J, et al. Remodeling of the connective tissue microarchitecture of the lamina cribrosa in early experimental glaucoma. *Invest Ophthalmol Vis Sci*. 2009;50:681–690.
70. Downs J, Roberts M, Burgoyne C, Hart R. Finite element modeling of the lamina cribrosa microstructure in normal and early glaucoma monkey eyes. *Invest Ophthalmol Vis Sci*. 2007;48:3301–3301.
71. Wang YX, Zhang Q, Yang H, Chen JD, Wang N, Jonas JB. Lamina cribrosa pore movement during acute intraocular pressure rise. *Br J Ophthalmol*. 2019 Sep 5. doi: 10.1136/bjophthalmol-2019-314016. [Epub ahead of print].
72. Zhang Q, Xu L, Wei WB, Wang YX, Jonas JB. Size and shape of Bruch's membrane opening in relationship to axial length, gamma zone, and macular Bruch's membrane defects. *Invest Ophthalmol Vis Sci*. 2019;60:2591–2598.
73. Goel M, Picciani RG, Lee RK, Bhattacharya SK. Aqueous humor dynamics: a review. *Open Ophthalmol J*. 2010;4:52.
74. Sigal IA, Grimm JL, Jan NJ, Reid K, Minckler DS, Brown DJ. Eye-specific IOP-induced displacements and deformations of human lamina cribrosa. *Invest Ophthalmol Vis Sci*. 2014;55:1–15.
75. Miller K. Constitutive model of brain tissue suitable for finite element analysis of surgical procedures. *J Biomech*. 1999;32:531–537.
76. Chan WH, Hussain AA, Marshall J. Youngs modulus of Bruch's membrane: implications for AMD. *Invest Ophthalmol Vis Sci*. 2007;48:2187–2187.

Investigative Ophthalmology & Visual Science